

Article

Evaluating the Efficiency of Connected and Automated Buses Platooning in Mixed Traffic Environment

Suyong Park ¹, Sanghyeon Nam ¹, Gokul S. Sankar ² and Kyoungseok Han ^{1,*} ¹ School of Mechanical Engineering, Kyungpook National University, Daegu 41566, Korea² Ford Motor Company, Dearborn, MI 48126, USA* Correspondence: kyoungsh@knu.ac.kr

Abstract: Due to the battery capacity limitation of battery electric vehicles (BEVs), the importance of minimizing energy consumption has been increasing in recent years. In the mean time, for improving vehicle energy efficiency, platooning has attracted attention of several automakers. Using the connected and automated vehicles (CAVs) technology, platooning can achieve a longer driving range while preserving a closer distance from the preceding vehicle, resulting in the minimization of the aerodynamic force. However, undesired behaviors of human-driven vehicles (HVs) in the platooning group can prohibit the maximization of the energy efficiency. In this paper, we developed a speed planner based on the model predictive control (MPC) to minimize the total platooning energy consumption, and HVs were programmed to maintain a long enough distance from the preceding vehicle to avoid collision. The simulations were performed to determine how HV influences the efficiencies of the platooning group, which is composed of CAVs and HVs together, in several scenarios including the different positions and numbers of the HVs. Test results show that the CAVs planned by our approach reduces energy consumption by about 4% or more than 4% compared to that of the HVs.

Keywords: platooning; connected and automated vehicle (CAV); electric bus; energy optimization; model predictive control



Citation: Park, S.; Nam, S.; Sankar, G.S.; Han, K. Evaluating the Efficiency of Connected and Automated Buses Platooning in Mixed Traffic Environment.

Electronics **2022**, *11*, 3231.

<https://doi.org/10.3390/electronics11193231>

electronics11193231

Academic Editors: Elías Revestido Herrero, Victor M. Becerra and Francisco Jesus Velasco

Received: 16 September 2022

Accepted: 3 October 2022

Published: 8 October 2022

Publisher's Note: MDPI stays neutral with regard to jurisdictional claims in published maps and institutional affiliations.



Copyright: © 2022 by the authors. Licensee MDPI, Basel, Switzerland. This article is an open access article distributed under the terms and conditions of the Creative Commons Attribution (CC BY) license (<https://creativecommons.org/licenses/by/4.0/>).

1. Introduction

Eco-friendly vehicles such as battery electric vehicles (BEVs) have been promoted to counter environmental issues, but their driving range is limited due to the limitation of the battery capacity [1,2]. Therefore, since the 20th century, the development of energy saving approaches to increase energy efficiency has attracted attention of many automakers. Some researchers have developed an optimal velocity planning scheme using traffic signal phase and timing (SPAT) [3,4], efficient regenerative braking systems to recharge batteries [5], and energy-efficient cabin climate control [6,7].

In addition, many researchers have proposed platooning using vehicle to everything (V2X) connection to improve energy efficiency [8–10]. The vehicles in platooning drive along the same trajectory, maintaining short inter-vehicle distance. The effect of improving energy efficiency and highway capacity can be achieved by platooning. To provide consistent signal coverage, a wireless communication infrastructure is necessary for vehicular communication. Vehicles exchange information about the local traffic conditions, and this advanced technology has led to the connected and automated vehicles (CAVs) [11–14]. This advancement can be exploited to form a group of vehicles that travel together to maximize energy efficiency. A small inter vehicle distance allows the platooning group to reduce the overall air resistance. For example, refs. [15,16] show how drag coefficient influences the energy consumption according to inter-vehicle distance. Depending on the number of vehicles, the air drag coefficient of vehicles in the group can be reduced by 40% [17]. This impact reduces the total air resistance of vehicles, thereby reducing energy consumption [18–20].

However, previous studies have not considered mixed CAVs and human-vehicles (HVs) in a specific platooning group. Communication between vehicles is difficult in this case because the HVs are disconnected from the CAVs. That is, the driving intention of HV is not unknown to CAV by nature. Evidently, for this disconnection, reducing the total air drag of the group is extremely grueling. From this motivation, in this paper, we develop an efficient energy platooning strategy for a group in which the CAVs and HVs coexist, and demonstrate the energy consumption results according to their formations.

Reinforcement learning (RL) is one of the theories to develop an eco-platooning strategy [21]. RL has an explosion of interest in technology to control automated vehicles, but learning-based algorithms may result in fatal accidents. Although dynamic programming (DP) can be considered, it requires the entire journey trajectory to calculate the optimal trajectory [22]. Therefore, DP cannot be implemented to real-time control. Meanwhile, model predictive control (MPC) can be considered as a solution to both safety and real-time issues. To predict optimal future the behavior, MPC calculates the trajectory of the future-modified inputs [23–26].

In this study, we exploit MPC and vehicle speed preview using V2X to plan energy efficiency platooning with mixed CAVs and HVs in the group. The main objective of this study is to create an optimized path for CAVs using the expected vehicle information. CAVs in platooning aim to reduce the overall energy consumption of the group. In addition, we analyzed how HVs affect energy consumption according to the platooning formation. The main contributions of this study are as follows:

(1) We propose the CAVs platooning control algorithm using MPC. Using predicted vehicle information, CAVs optimize speed trajectory to minimize the total platooning energy consumption, and the effectiveness is confirmed through simulations under various conditions.

(2) We analyze the energy consumption with respect to platooning formation mixed with HVs. Although HVs are disconnected with CAVs, we estimate the HVs behavior to keep short distance from the preceding vehicle as much as possible to minimize air resistance.

The rest of this paper is organized as follows. In Section 2, we define the problem formulation for the case of mixed CAVs and HVs for platooning. In Section 3, we present the simulation modeling for the electric bus, and compare vehicle model from Autonomie with the control-oriented model. Autonomie [27] offers a reliable model and a small discrepancy with the test results. In Section 4, we present a platooning strategy that minimize energy consumption. In Section 5, we introduce the intelligent driving model (IDM) for HV model and estimate the behavior of a HV using a particle filter. The simulation results are discussed in Section 6 followed by the summary and conclusions in Section 7.

2. Problem Formulation

Figure 1 depicts an illustration of the platooning scenario. Leading vehicle is considered as a CAV in platooning for complete communication links. We assume that CAVs are connected to predecessor-leader-following (PLF) communication [28]. Owing to its complete communication links, the PLF communication topology performs better than the others, leading to the prediction of the future CAV behavior. This advantage allows us to adapt MPC to optimize path planning. Nevertheless, CAVs are connected to each other, whereas HVs are disconnected from CAVs. This implies that HVs cannot provide the predicted behavior. In this study, we assume that the HV position can be detected with noise and we propose the estimation of HVs speed using a particle filter. We used this information to maintain a short inter-vehicle distance from the preceding HV. The measurement of inter-vehicle distance is an important issue for the safety and reduction of air resistance in platooning [29].

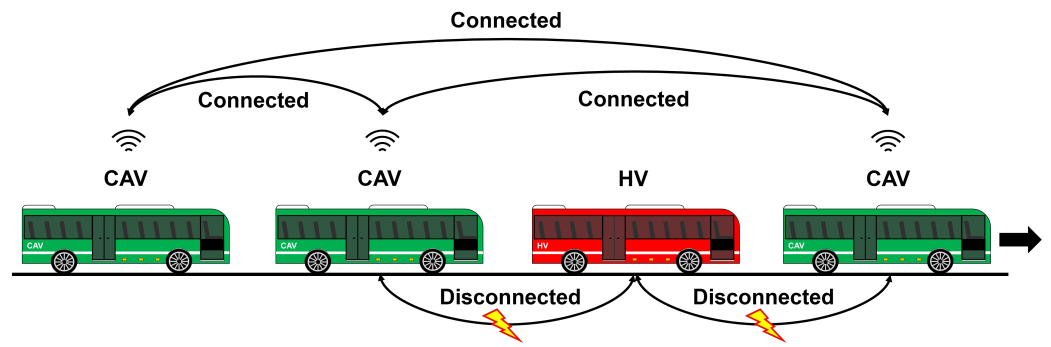


Figure 1. Illustration of the platooning scenario. CAVs are connected each other by using V2X technologies while human-vehicle(HV) disconnected with CAVs.

3. System Modeling

3.1. Vehicle Longitudinal Dynamics

As shown in Figure 2, in this subsection, the longitudinal dynamics of the vehicle are described. In this study, we assume that vehicles only drive in a longitudinal direction. The disturbances like cut-in and the lane-changing maneuver is not considered. The vehicle longitudinal dynamics is as follows.

$$\dot{s} = v \tag{1}$$

$$\dot{v} = \frac{T_w}{mr} - \frac{1}{2m} \rho A C_d C_f v^2 - g \sin \theta - f g \cos \theta \tag{2}$$

where s denotes travel distance of the vehicle, v denotes the vehicle speed, T_w denotes the applied input wheel torque, m denotes the vehicle mass, r denotes the wheel radius, ρ denotes the air density, A is the frontal area of the vehicle, g denotes the constant as gravity, θ denotes the road slope, f is the rolling resistance coefficient, C_d is the drag coefficient, and C_f is the drag coefficient ratio.

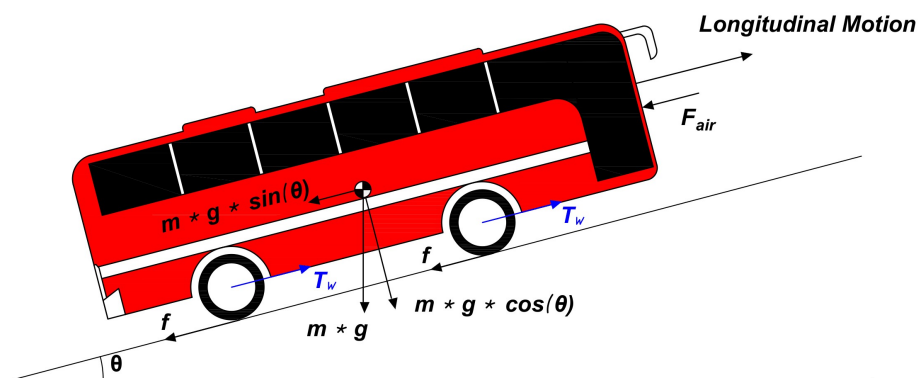


Figure 2. Longitudinal vehicle dynamics.

The control input, i.e., motor torque T_m , is calculated as follows:

$$T_m \approx \frac{T_w}{i_0} \tag{3}$$

where T_w denotes the input wheel torque and i_0 denotes the final reduction gear ratio.

In general, the air resistance of individual vehicles in platoons is affected by the distance between vehicles. The numerical analysis done by Zabat et al. [30] measured aerodynamic drag coefficients of light-duty vehicles (LDVs) in the wind tunnel. The results show that shorter vehicle spaces in platoons present a reduced average drag coefficient. The average drag reduction showed up to 55% for five-vehicle platoon at inter-vehicle

distance 5 m [31]. Through the drag coefficient ratio C_f multiplied by aerodynamic force, the control-oriented model can be more accurate to find optimal control action. We refer Hussein et al. [32] which proposes fitting drag coefficient ratio, using rational polynomial function based on experiment measurement, and C_f is defined as follows:

$$C_f = \begin{cases} \frac{a_n d_{inter}^n + a_{n-1} d_{inter}^{n-1} + \dots + a_1 d_{inter}^1 + a_0}{b_n d_{inter}^n + b_{n-1} d_{inter}^{n-1} + \dots + b_1 d_{inter}^1 + b_0}, & 0 < G \leq G_0 \\ 1, & G \geq G_0 \end{cases} \quad (4)$$

Here C_f is the drag coefficient ratio between the ego car and the preceding car, d_{inter} is the distance gap, a_n and b_n are calibrated constants, and n denotes the number of vehicles in the convoy.

If a single vehicle in the platoon exceeds the critical inter-vehicle distance G_0 , the vehicle is not susceptible to the drag coefficient ratio (i.e., $C_f = 1$). Therefore, the inter-vehicle distance of a single vehicle must be less than G_0 in order to take advantage of the drag coefficient ratio's benefit. The ego vehicle's C_f is calculated using d_{inter} between the ego and its preceding vehicle at time k . d_{inter} at time k can be calculated as follows:

$$d_{inter} = d_p - d_e \quad (5)$$

where d_p is the preceding car's and d_e is the ego car's inter-vehicle distance.

As shown in Figure 3, actual and approximated drag coefficient ratio C_f data set for three-buses in platoons is depicted. The drag coefficient ratio of individual vehicles in platoon increases exponentially until inter-vehicle distance approaches critical point G_0 . Although C_f can be minimized as d_{inter} approaches zero, we specify the minimum d_{inter} value to keep the safety. In addition, it is assumed that the third car in the platoon's drag reduction is the same from the perspective of the vehicle behind it. This model was developed by [32] and was obtained using empirical dataset [33]. The parameters data empirically fitted for C_f are listed in Table 1.

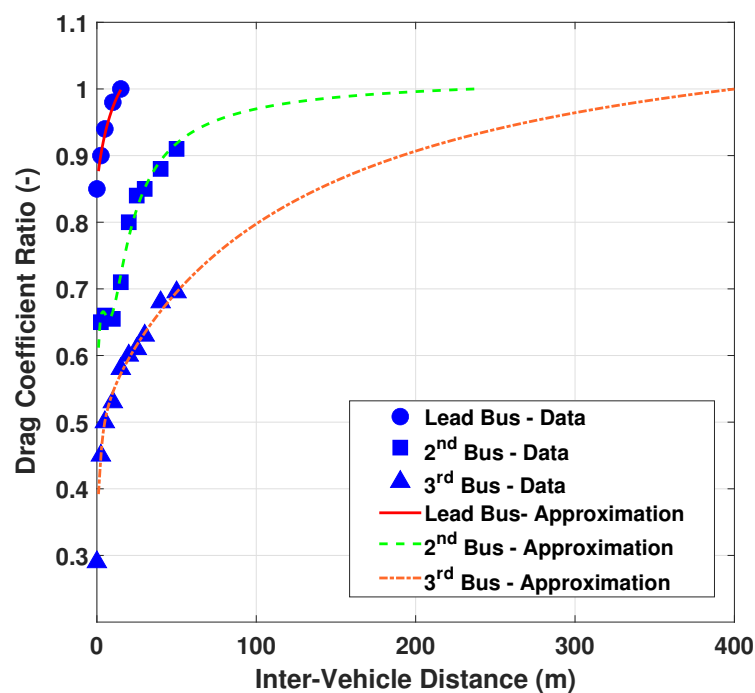


Figure 3. Drag coefficient ratio C_f for three-bus in platoons according to inter-vehicle distance. The fitting parameters of the drag coefficients ratio is presented by [32] based on actual data [33].

Table 1. Parameters of the drag coefficients ratio for individual bus platoons [32].

| Parameters | Bus Platoon | | | | |
|------------|--------------------------|--------------------------|--------------------------|-----------------------|-------------------------|
| | Two Buses | | Three Buses | | |
| | Lead | Trail | Lead | Middle | Trail |
| a_3 | -1.5175×10^{-4} | -7.2951×10^{-4} | -1.5175×10^{-4} | 4.7945×10^3 | 9.3348×10^{-2} |
| a_2 | 1.3115×10^{-1} | 4.4369×10^{-1} | 1.3115×10^{-1} | -4.0404×10^4 | 5.1656 |
| a_1 | 1.5396 | 6.1509 | 1.5369 | 3.5213×10^5 | -3.9662 |
| a_0 | 3.4243×10^{-1} | 1.1174×10 | 3.4243×10^{-1} | 1.0311×10^6 | 6.7697 |
| b_3 | -8.9422×10^{-5} | -8.5027×10^{-4} | -8.9422×10^{-5} | 4.6933×10^3 | 8.1124×10^{-2} |
| b_2 | 1.1463×10^{-1} | 4.6002×10^{-1} | 1.1463×10^{-1} | -1.6202×10^4 | 1.0062×10 |
| b_1 | 1.7730 | 1.2569×10 | 1.7730 | 2.9853×10^5 | -4.2684 |
| b_0 | 4.0877×10^{-1} | 1.9639×10 | 4.0877×10^{-1} | 1.9158×10^6 | 1.4692×10 |
| G_0 | - | 3.0815×10^2 | - | 2.4082×10^2 | 4.0045×10^2 |

3.2. Battery Dynamics

In this subsection, we introduce the battery dynamics to calculate required energy to generate the vehicle traction force. The battery state of charge (SOC) is as follows:

$$SOC(t) = SOC(t_0) - \frac{\int_{t_0}^t I_b(t)dt}{C} \tag{6}$$

where I_b denotes the battery current, and C is the battery maximum capacity.

The SOC is estimated based on battery current condition. The battery current I_b is calculated as follows:

$$I_b(t) = \frac{P_b(t)}{V(t)} \tag{7}$$

where P_b is the battery power, and V denotes the battery voltage. The battery is discharged when P_b is positive, and charging when P_b is negative. The P_b expressed described as follows:

$$P_b = \begin{cases} P_m e_b, & P_m < 0 \\ \frac{P_m}{e_b}, & P_m \geq 0 \end{cases} \tag{8}$$

where P_m is the motor power, which is positive when motor power is used to produce traction force, and e_b is the battery efficiency. To obtain P_m , we used a look-up table indexed by the motor speed and torque (see Figure 4).

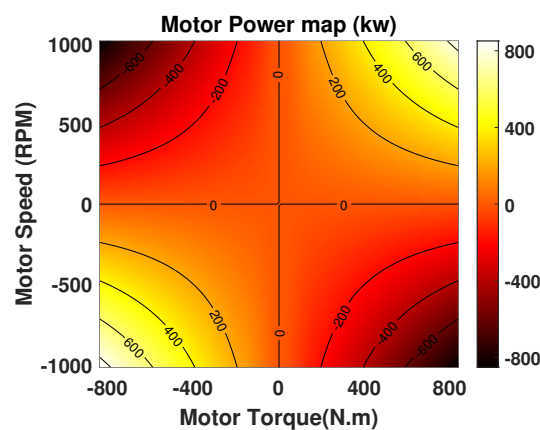


Figure 4. Motor power map indexed by motor torque and speed.

As shown in Figure 5, the control-oriented and Autonomie models are compared. The simulation results [27] show the accuracy of the vehicle model provided by Autonomie. In this study, the simulation was implemented by using the UDDS velocity profile and the parameters of the vehicle model are listed in Table 2. The discrepancy in the SOC between the control oriented model and the Autonomie is 1.75%. Through this simulation, we developed a reliable vehicle model for electric buses.

Table 2. Electric-bus parameter values offered from AMBER [34].

| Description | Symbol | Value |
|-----------------------------------|--------|-----------------------------|
| Mass of the vehicle | m | 19,717 [kg] |
| Wheel radius | r | 0.4655 [m] |
| Ratio for single reduction gear | i_0 | 11.76 [-] |
| Frontal area | A_f | 7.33 [m ²] |
| Coefficient of rolling resistance | f | 0.00863 [-] |
| Drag coefficient | C_d | 0.65 [-] |
| Battery voltage | V | [3.5 4.2] [V] |
| Battery efficiency | e_b | 0.9 [-] |
| Maximum capacity of battery | C_b | 33.1 [Ah] |
| SOC range | SOC | [0 1] [-] |
| Gravity | g | 9.81 [m/s ²] |
| Air density | ρ | 1.1985 [kg/m ³] |

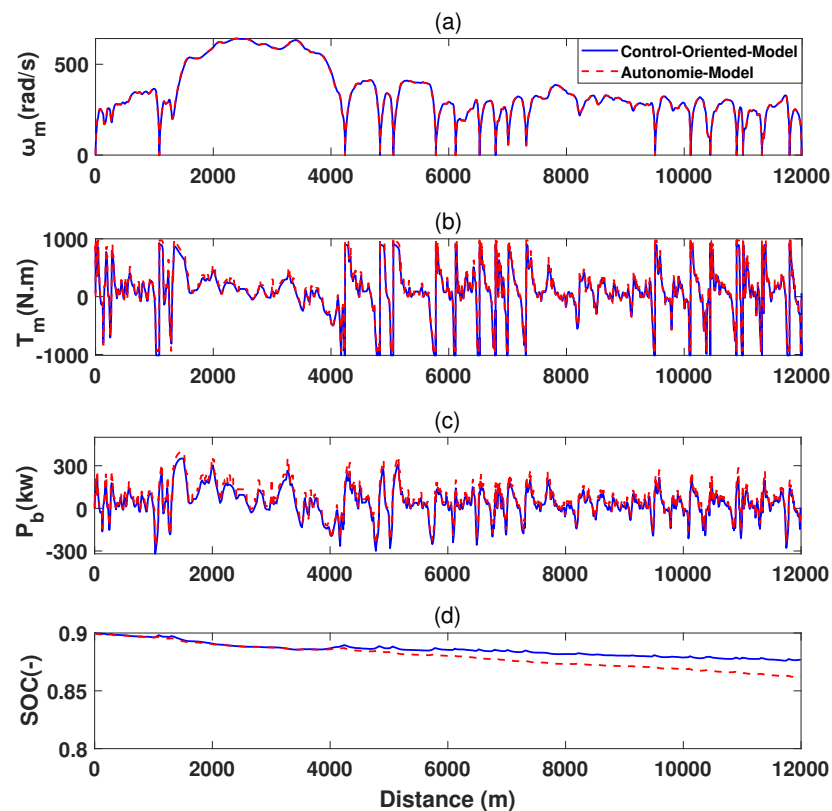


Figure 5. The driving results of the control oriented-model and the AMBER model are compared. (a) Motor speed (ω_m), (b) Motor torque (T_m), (c) Battery power (P_b), (d) State of Charge (SOC).

4. Nonlinear Programming Problem

The optimal control was designed to minimize the energy consumption. The key idea of our approach is to maximize regenerative braking and minimize air resistance by considering highway road information. We propose the design of the cost function and control constraints for the prediction and control horizon N :

$$\min_{u \in U} \sum_{k=0}^{N-1} W_1 P_b(k|i) + W_2 C_f(k|i) \tag{9a}$$

subject to

$$T_m^{\min} < u(k|i) < T_m^{\max} \tag{9b}$$

$$d_{inter}^{\min} < d_{inter}(k+1|i) < d_{inter}^{\max} \tag{9c}$$

$$v^{\min}(k+1|i) < v(k+1|i) < \eta \cdot \hat{v}^p(k+1|i) \tag{9d}$$

$$k = 0, 1, 2 \dots, N - 1,$$

where W_1, W_2 is the weight factor, $[T_m^{\min}, T_m^{\max}]$ is the restricted range of control input, and $[d_{inter}^{\min}, d_{inter}^{\max}]$ is the predefined range of the inter-vehicle distance while avoiding vehicle collisions and reducing the drag coefficient. η is a safety variable, \hat{v}^p denotes preceding vehicle velocity and $i+k$ is obtained at time instant i . We tuned W_1, W_2 factors according to road information to maximize energy efficiency.

5. Car-Following Model and Velocity Estimation

In this section, we introduce an intelligent driver model (IDM) to model collision-free car following motion. Since the communication between HVs and CAVs is not available, the behavior of HV is highly uncertain. For this reason, the CAV following the HV employs the IDM because using the MPC with predicted information is not available. Also, a particle filter is used to estimate the HV's velocity using the sensor measurements [35,36].

5.1. Intelligent Driving Model

The IDM model can adjust the desired safety time gap and the longitudinal velocity [37]. The IDM model is given by

$$\dot{v}(t) = a \left[1 - \left(\frac{v(t)}{v_0} \right)^\delta - \left(\frac{s^*(v, \Delta v)}{s(t)} \right)^2 \right] \tag{10}$$

where a denotes the maximum acceleration, v_0 denotes the preferred velocity, and $s^*(v, \Delta v)$ denotes the desired gap. The desired gap $s^*(v, \Delta v)$ is given by

$$s^*(v, \Delta v) = s_0 + s_1 \sqrt{\frac{v}{v_0}} + T_h v + \frac{v \Delta v}{2\sqrt{ab}} \tag{11}$$

where s_0 and s_1 are the minimum gap when following other vehicles, T_h denotes time headway, and b denotes the characterized deceleration.

5.2. Particle Filter-Based Velocity Estimation

In this subsection, we propose a method of estimating HV's velocity using particle filter (a.k.a. sequential Monte Carlo) in order to keep the safe-distance while following. Since HV drives stochastically at every moment, we should estimate HV's velocity through a probability-based particle filter. The basic principle of the particle filter is well described in [38].

It is assumed that the preceding HV's position is measured continuously and this position information is used to estimate the HV's state variable x_{k+1} . The current state x_k is calculated by the measurement during the sampling time. The distribution of particles should be conducted because the future HV's behavior is predicted based on probability. For this reason, we randomly scattered particles to find the behavior of HV that most likely to happen. The distribution is calculated as follows.

$$x_{k+1,i} = f_k(x_{k,i}, w_k) \quad i = 1, \dots, N \tag{12}$$

where k indicates the time instance, x_k is the state variable, w_k is the process noise, T_s is the sampling time, z_k is the measurement noise, i is the index for the particle, and N is the

number of particles generated via trial-and-error. We randomly generate N particles $x_{k,i}$ at time k . In this process, white noise w_k that is randomly generated is considered to prevent the case that particles are distributed on the point which is much far from the actual data.

Subsequently, we weight the particles based on relative likelihood to approximate actual velocity. The relative likelihood $q_{k,i}(x_{k,i})$ is assumed to be followed the Gaussian distribution:

$$q_{k,i}(x_{k,i}) = \frac{1}{(2\pi R)^{1/2}} \exp\left(\frac{-(x_k^* - x_{k,i})^2}{2R}\right) \tag{13}$$

where x_k^* is the estimated state variable at time instance k , and R is the variance.

We define a new distribution of cumulative probability function(CDF) for the resampling step. The CDF can prevent being biased by considering the only one points that lots particles are gathered when the resampling happens. The normalized relative likelihood can be expressed as follows:

$$q_i = \frac{q_i}{\sum_{j=1}^N q_j} \tag{14}$$

The resampling stage was conducted q_i into the accumulated distribution. Based on the accumulated distribution, sum of all the normalized relative likelihood is equal to one. We randomly pick particles given weight and average them for estimation. The approximated mean of particles is given by

$$E(x_{k+1}) \approx \frac{1}{N} \sum_{i=1}^N x_{k,i} \tag{15}$$

where $E(x_k)$ denotes the expected value.

The particle $x_{k,i}$ is randomly selected in the accumulated distribution domain q_i for resampling. Subsequently, the sum of the resampled particles $x_{k,i}$ is divided by the number of particles to calculate the expectation value. We set x_k as HV's velocity to keep safty distance.

As shown in Figure 6, the estimation of HV speed is depicted when it is driven based on the adapted US06 speed profile. We assumed that the HV position and state are the HV velocities. Although there are some differences between the actual and estimated data, the estimation tracks the intended acceleration and deceleration of human vehicles. Using the estimated value, the vehicle behind the HV was followed by using the IDM model.

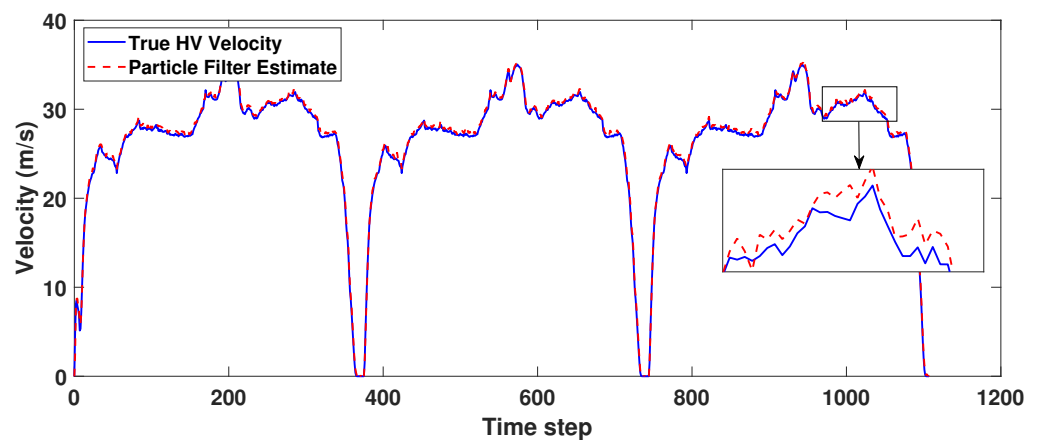


Figure 6. Particle filter results in human vehicle driving based on three-times US06 speed profile.

6. Simulation and Results

In this section, we evaluate developed CAV speed planner in various scenarios in terms of the energy efficiency according to the HVs position and the number of HVs. We

assumed that all the leading vehicles in the scenario drive with a modified US06 speed profile in highway. The total travel distance for the leading vehicle is 29.78 km, and speed profile of the leading vehicle is shown in Figure A3. In addition, road slope information was obtained from Google Earth [39] (see Figure A1). The following vehicles travel until the leading vehicle stops. The simulation is performed in Windows 10 operating system with Intel(R) Core(TM) i5-9500, 16GB RAM memory. The MPC problem is solved by MATLAB function *fmincon()*.

6.1. Case 1: Energy Efficiencies Depending on the Locations of HV on the Flat Road

In this subsection, four scenarios were considered, as shown in Figure 7 in which the leading CAV is assumed to drive with deformed US06 speed profile on the flat road, so the total travel distance for the leading vehicle was 29.78 km. Scenarios 1, 2, 3, and 4 are illustrated in which the HV is placed differently. Figure 8 shows the average gap and the reduced drag coefficient factor C_f between the preceding and following vehicles for each scenario. The red, green, and orange bars indicate the HV, CAV, and average values, respectively.

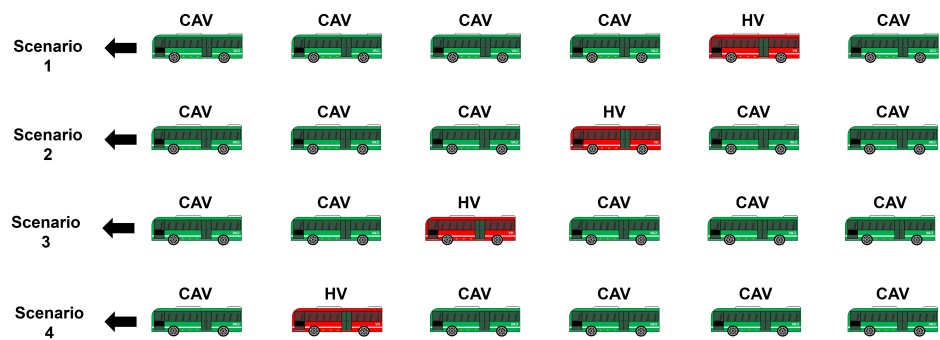


Figure 7. Platooning scenario according to the location of HV.

As discussed in Table 3, where the aero drag coefficient decreases if the more vehicles travel in front even if the inter-distance between vehicles are same, the HV in the scenario 1 consumed more average SOC than other scenario. It is observed that the position of vehicle strongly influences on the energy consumption. Although HVs drive with similar inter-vehicle distance, drag coefficient is applied differently depending on the position (see Figure 3). As shown in Figure 8, the HV in the scenario 1 has the most biggest drag coefficient 0.91 which consumes the most battery energy.

Table 3. Battery SOC consumption for four scenarios in Case 1.

| Scenario | 1st Bus SOC (%) | 2st Bus SOC (%) | 3st Bus SOC (%) | 4st Bus SOC (%) | 5st Bus SOC (%) | 6st Bus SOC (%) | Average SOC Consumption (%) |
|------------|-----------------|-----------------|-----------------|-----------------|-----------------|-----------------|-----------------------------|
| Scenario 1 | 22.97 | 22.07 | 20.98 | 18.21 | 17.97 | 17.99 | 20.03 |
| Scenario 2 | 22.97 | 19.92 | 20.13 | 20.6 | 18.02 | 17.96 | 19.80 |
| Scenario 3 | 22.97 | 19.32 | 18.15 | 20.15 | 20.68 | 17.99 | 19.84 |
| Scenario 4 | 22.97 | 19.12 | 18.15 | 18.08 | 20.01 | 20.47 | 19.98 |

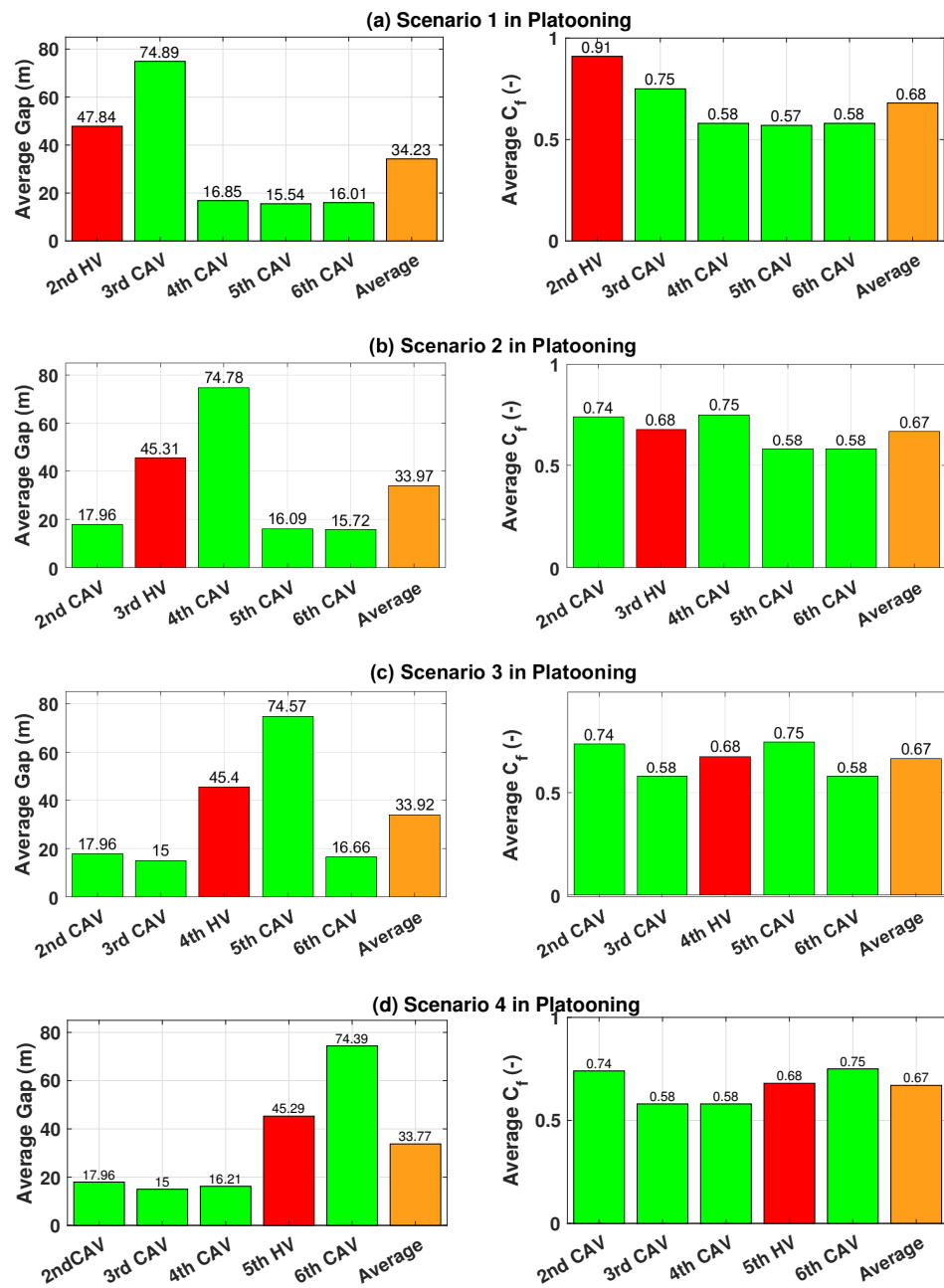


Figure 8. Average inter-vehicle distance and drag coefficient ratio under scenarios 1, 2, 3 and 4 in Case 1. Red: HV; Green: CAV; Orange: Average.

6.2. Case 2: Energy Efficiencies Depending on the Locations of HV on the Sloped Road

In this subsection, we analyze the energy efficiencies for each scenario on the sloped road (see Figure 7). Test results of each scenario’s SOC consumptions are described in Table 4. The SOC of CAVs following HV is higher than other vehicles. This results are caused by (9), where the vehicles use the regenerative braking function as much as possible, which is more effective than reducing drag coefficient on sloped road. In the Figure 9, CAV that located right behind of human vehicle has shorter inter-vehicle distance from the preceding car compared to other CAVs in every scenarios which have high drag coefficient. However, the SOC of CAVs which drive with long inter-vehicle distance was lower than others even though they have bigger air drag coefficients. To sum up, we can conclude that energy recovering by the regenerative braking is more effective than the reducing aero drag coefficient.

Table 4. Battery SOC consumption for four scenarios in Case 2.

| Scenario | 1st Bus SOC (%) | 2nd Bus SOC (%) | 3rd Bus SOC (%) | 1st Bus SOC (%) | 5th Bus SOC (%) | 6th Bus SOC (%) | Average SOC Consumption (%) |
|------------|-----------------|-----------------|-----------------|-----------------|-----------------|-----------------|-----------------------------|
| Scenario 1 | 23.33 | 22.55 | 20.98 | 19.96 | 19.79 | 19.99 | 21.17 |
| Scenario 2 | 23.33 | 20.21 | 20.81 | 21.20 | 19.78 | 20.01 | 20.99 |
| Scenario 3 | 23.33 | 20.21 | 19.80 | 20.65 | 21.03 | 19.93 | 20.93 |
| Scenario 4 | 23.33 | 20.21 | 19.80 | 19.78 | 20.71 | 21.16 | 20.94 |

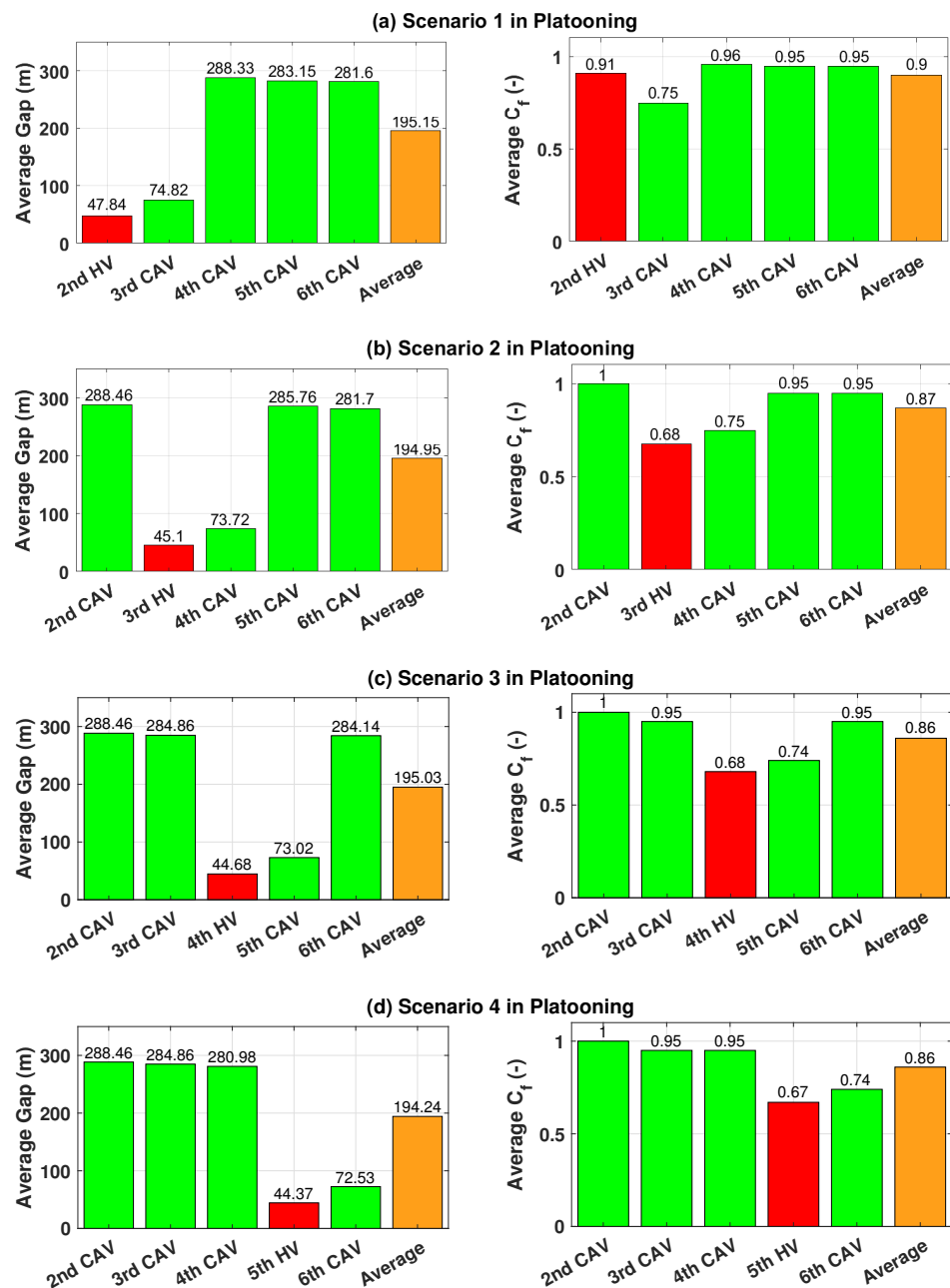


Figure 9. Average inter-vehicle distance and drag coefficient ratio under scenarios 1, 2, 3 and 4 in Case 2. Red: HV; Green: CAV; Orange: Average.

6.3. Case 3: Energy Efficiencies Depending on the Number of Multiple HVs on a Flat Road

In this section, scenarios 5, 6, 7 and 8 are considered as shown in Figure 10. Each scenario has the different number of the HV and results show how that influenced to the platooning group. As shown on the Table 5, the average SOC consumption results show that as the number of the HV increases, the average energy consumption tends to increase.

The scenario 8 with the most number of HVs consumed an average SOC 21.23%, whereas 20.03% average SOC is consumed in Scenario 5 which has the fewest number of HVs. As shown in Figure 11, CAVs have lower drag than HVs because CAVs can maintain shorter inter-vehicle distance. The result of scenario 8 shows that scenario 8 has a higher average inter-vehicle distance than scenario 7, which leads to higher air resistance. Overall, more CAVs deployed in platoon can save energy consumption.

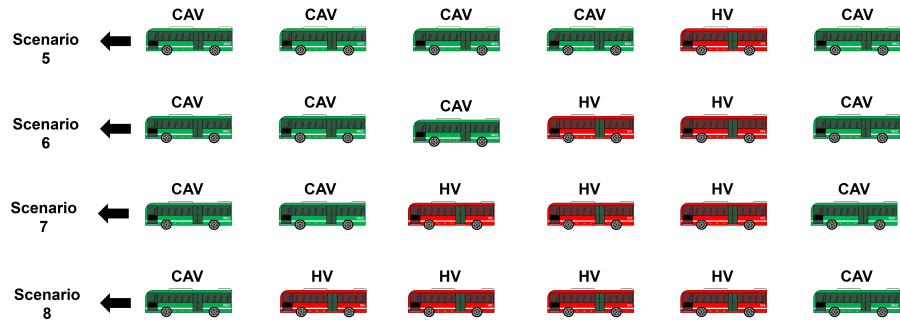


Figure 10. Platooning scenario according to the number of multiple HVs.

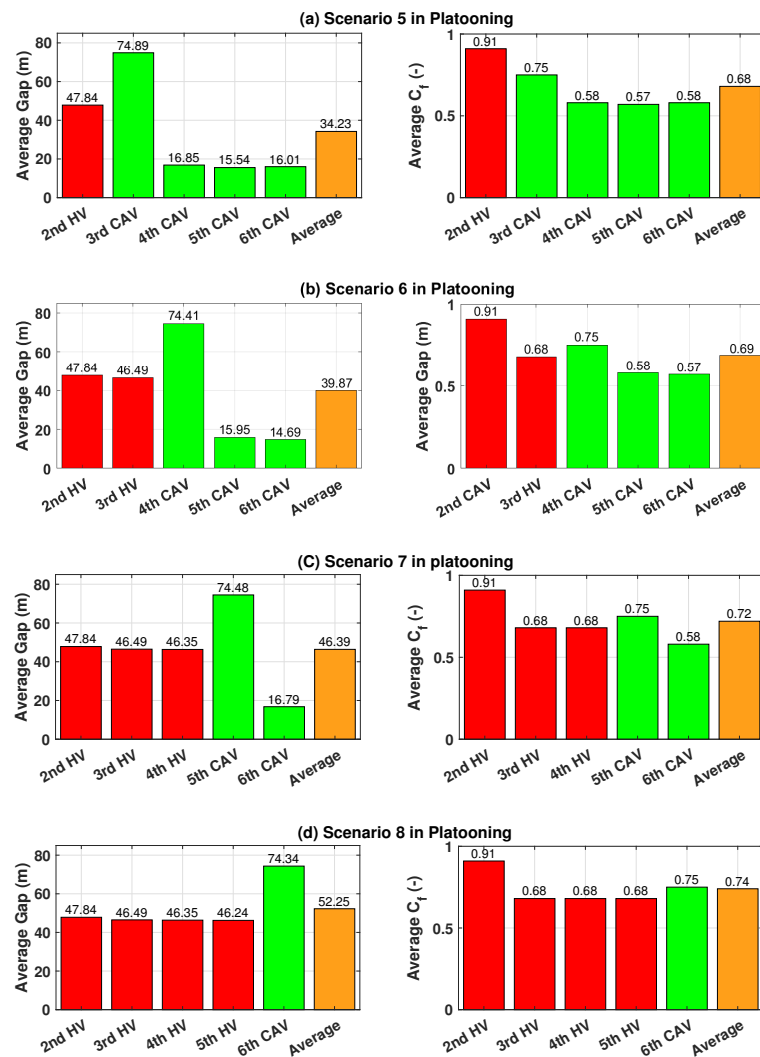


Figure 11. Average inter-vehicle distance and drag coefficient ratio under scenarios 5,6,7 and 8 in Case 3. Red: HV; Green: CAV; Orange: Average.

Table 5. Battery SOC consumption for four scenarios in Case 3.

| Scenario | 1st Bus SOC (%) | 2nd Bus SOC (%) | 3rd Bus SOC (%) | 4th Bus SOC (%) | 5th Bus SOC (%) | 6th Bus SOC (%) | Average SOC Consumption (%) |
|------------|-----------------|-----------------|-----------------|-----------------|-----------------|-----------------|-----------------------------|
| Scenario 5 | 22.97 | 22.07 | 20.98 | 18.21 | 17.97 | 17.99 | 20.03 |
| Scenario 6 | 22.97 | 22.07 | 20.47 | 22.06 | 17.99 | 17.90 | 20.58 |
| Scenario 7 | 22.97 | 22.07 | 20.47 | 20.46 | 20.97 | 18.15 | 20.85 |
| Scenario 8 | 22.97 | 22.07 | 20.47 | 20.46 | 20.44 | 20.98 | 21.23 |

6.4. Case 4: Energy Efficiencies Depending on the Number of Multiple HVs on the Sloped Road

In this subsection, we analyze the energy efficiencies for each scenario on the sloped road (see Figure 10). Each scenario has the different number of the HV and test results show how the number of HVs between CAVs influence the energy efficiency of the vehicle group. As the number of HVs increased, the average SOC consumption also increases as depicted in Table 6. This is because more CAVs in platoon can save energy consumption while exploiting regenerative brake. Although the average gap and C_f in scenario 5 were higher than other scenarios, they consumed lesser energy than other scenarios as shown in Figure 12. This implies that exploiting regenerative brake is more effective than reducing the air resistance on the sloped road from the perspective of saving energy.

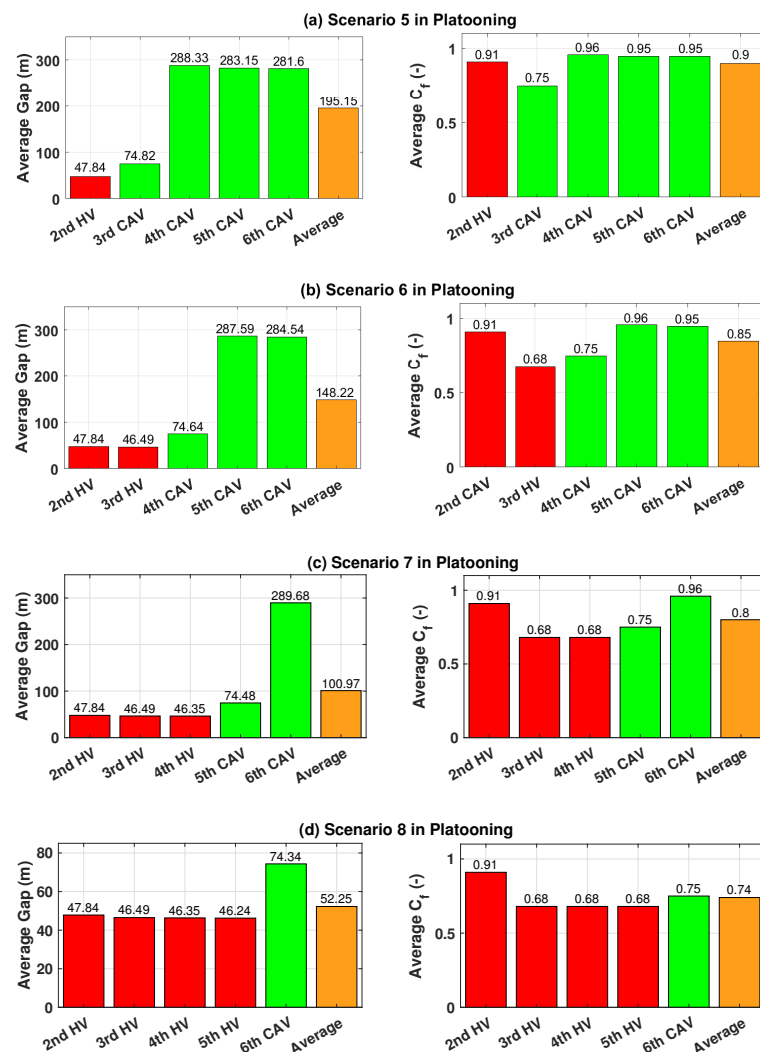


Figure 12. Average inter-vehicle distance and drag coefficient ratio under scenarios 5, 6, 7 and 8 in case 4. Red: HV; Green: CAV; Orange: Average.

Table 6. Battery SOC consumption for four scenarios in Case 4.

| Scenario | 1st Bus SOC (%) | 2st Bus SOC (%) | 3st Bus SOC (%) | 4st Bus SOC (%) | 5st Bus SOC (%) | 6st Bus SOC (%) | Average SOC Consumption (%) |
|------------|-----------------|-----------------|-----------------|-----------------|-----------------|-----------------|-----------------------------|
| Scenario 5 | 23.33 | 22.55 | 20.98 | 19.96 | 19.79 | 19.99 | 21.1 |
| Scenario 6 | 23.33 | 22.55 | 21.05 | 21.58 | 19.89 | 19.85 | 21.32 |
| Scenario 7 | 23.33 | 22.55 | 21.05 | 21.01 | 21.51 | 19.93 | 21.56 |
| Scenario 8 | 23.33 | 22.55 | 21.05 | 21.01 | 20.99 | 21.57 | 21.75 |

7. Conclusions

In this paper, we propose the energy-efficient control framework for CAV in platoon and evaluate its effectiveness in mixed traffic environment. Especially, using the connectivities, the vehicles future behaviors are exploited when optimizing the velocity profiles of multiple CAVs.

The two main distinctions of this study compared to existing studies are as follows. First, the MPC-based controller for CAVs performed better than that for HVs in terms of energy efficiency. Second, we propose estimating HV's velocity through a probability-based particle filter. The CAVs use estimated HV's velocity to keep the safety distance while HV drives stochastically at every moment. An evaluation is performed to verify our approach under various platooning scenarios. The 5th CAV saved energy consumption by up to 4.1% compared to HV in scenario 5. In addition, as the number of HVs in a group increases, the average battery SOC consumption decrease. The average battery SOC consumption value differed by up to 1.2% depending on the number of HVs in the convoy. However, the average battery SOC consumption according to the position of the HV does not have a meaningful relationship. This is because our predefined HV travels with a reasonable inter-vehicle distance from the preceding vehicle, which can reduce energy consumption. Our approach shows that CAV only use HV's estimated information to keep a safety distance.

In future studies, we will model the human-drivers with different driving characteristics, then we will perform hardware-in-loop (HIL) test to verify the applicability of our approach in the mixed-traffic environment in real-time.

Author Contributions: Conceptualization, S.P. and K.H.; methodology, S.P. and K.H.; software, S.P. and S.N.; validation, S.P., S.N., G.S.S. and K.H.; formal analysis, S.P.; investigation, S.P.; resources, S.P.; data curation, S.P.; writing—original draft preparation, S.P. and S.N.; writing—review and editing, S.P., S.N., G.S.S. and K.H.; supervision, K.H. All authors have read and agreed to the published version of the manuscript.

Funding: This research was supported in by Basic Science Research Program through the National Research Foundation of Korea (NRF) funded by the Ministry of Education (No. NRF-2021R1A6A1A0304 3144); in part by the BK21 funded by the Ministry of Education, Korea (4199990314305), and in part by the Technology Innovation Program ('20021926', 'Development of Eco-friendly Vehicle Tuning Supported Open Platform using Design and Verification Technology for Carbon Neutrality', '20014121', 'Industrial Strategic Technology Development Program-Development of Integrated Minimal Risk Maneuver Technology for Fallback system during Autonomous Driving') funded by the Ministry of Trade, Industry & Energy (MOTIE, Korea).

Conflicts of Interest: The authors declare no conflict to interest.

Appendix A

The road slope information was provided from Google Earth, as shown in Figure A1. We assumed that the leading vehicle traveled Daegu to Busan on a highway in south korea as shown in Figure A2. In this study, the lateral position was not considered. This implies that platooning only drives in a longitudinal direction, and there is no lane-changing.

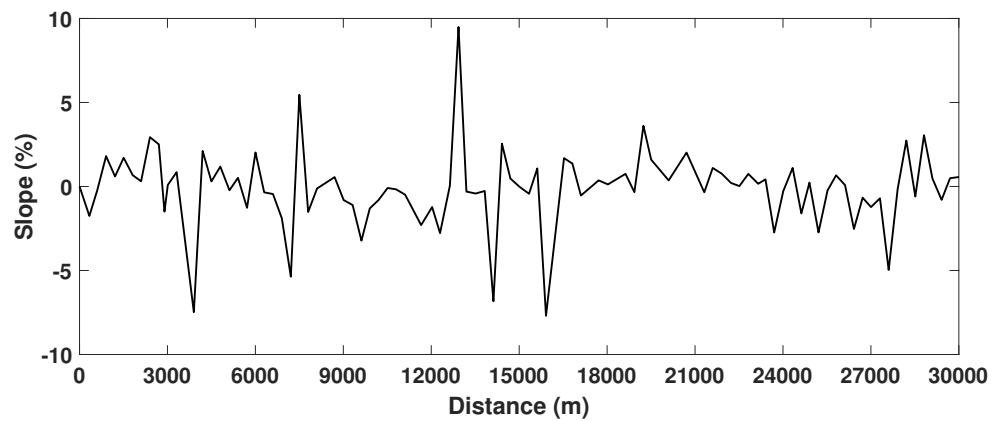


Figure A1. Road slope information of the certain period between Daegu and Busan in South Korea (Google Earth).

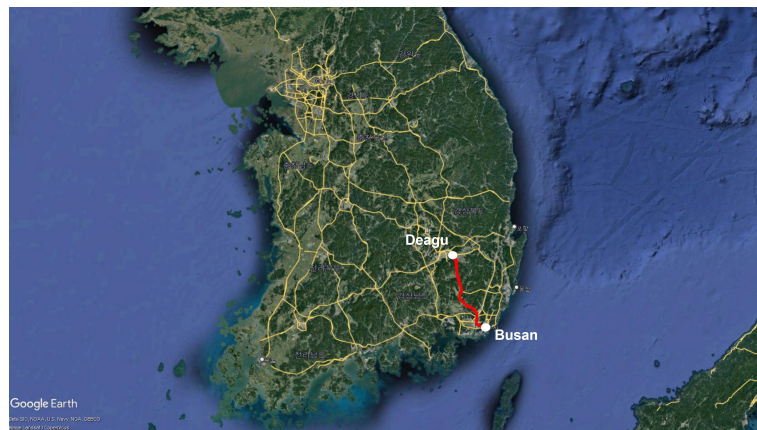


Figure A2. Expressway information from Daegu to Busan in South Korea (Google Earth).

Appendix B

As shown in Figure A3, the leading vehicle travels with a deformed US06 speed profile. This is because the acceleration ability of the BEV electric bus is a burden for following the US06 speed profile. We only considered a section with a high speed range in US06. The total travel distance is 29.78 km on a highway.

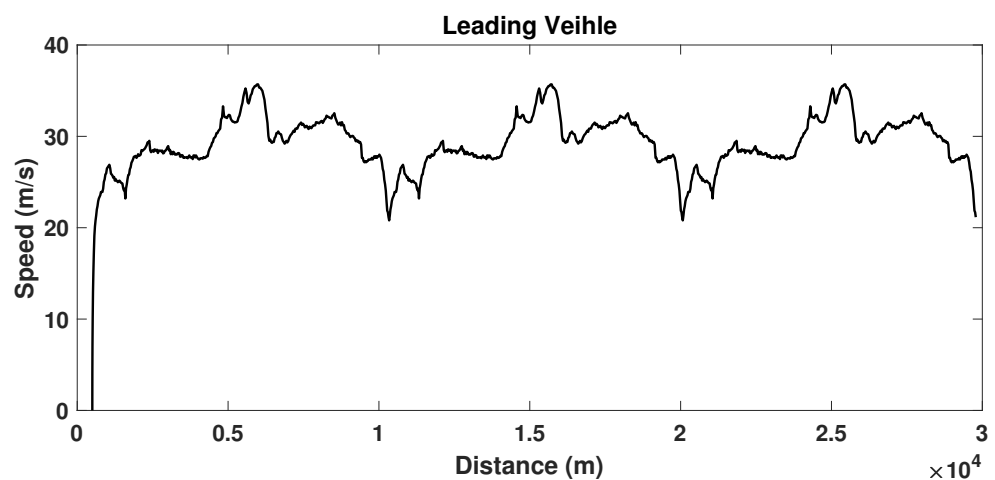


Figure A3. Leading vehicles traveling with deformed US06 speed profile.

References

1. Tran, M.-K.; Bhatti, A.; Vrolyk, R.; Wong, D.; Panchal, S.; Fowler, M.; Fraser, R. A review of range extenders in battery electric vehicles: Current Progress and Future Perspectives. *World Electr. Veh. J.* **2021**, *12*, 54. [CrossRef]
2. Lain, M.J.; Kendrick, E. Understanding the limitations of lithium ion batteries at high rates. *J. Power Sources* **2021**, *493*, 229690. [CrossRef]
3. Mahler, G.; Vahidi, A. An optimal velocity-planning scheme for vehicle energy efficiency through probabilistic prediction of traffic-signal timing. *IEEE Trans. Intell. Transp. Syst.* **2014**, *15*, 2516–2523. [CrossRef]
4. Han, J.; Shen, D.; Karbowski, D.; Rousseau, A. Leveraging multiple connected traffic light signals in an energy-efficient speed planner. *IEEE Control. Syst. Lett.* **2021**, *5*, 2078–2083. [CrossRef]
5. Wu, J.; Wang, X.; Li, L.; Qin, C.; Du, Y. Hierarchical control strategy with battery aging consideration for hybrid electric vehicle regenerative braking control. *Energy* **2018**, *145*, 301–312. [CrossRef]
6. Chen, Y.; Kwak, K.H.; Kim, J.; Kim, Y.; Jung, D. Energy-efficient cabin climate control of electric vehicles using linear time-varying model predictive control. In *Optimal Control Applications and Methods*; Wiley: Hoboken, NJ, USA, 2021.
7. Shuofeng, Z.; Amini, M.R.; Sun, J.; Mi, C. A two-layer real-time optimization control strategy for Integrated Battery Thermal Management and HVAC system in connected and automated hevs. *IEEE Trans. Veh. Technol.* **2021**, *70*, 6567–6576. [CrossRef]
8. Wang, C.; Dai, Y.; Xia, J. A CAV platoon control method for isolated intersections: Guaranteed feasible multi-objective approach with priority. *Energies* **2020**, *13*, 625. [CrossRef]
9. Pearre, N.S.; Ribberink, H. Review of research on V2X technologies, strategies, and operations. *Renew. Sustain. Energy Rev.* **2019**, *105*, 61–70. [CrossRef]
10. Storck, C.R.; Duarte-Figueiredo, F. A 5G V2X ecosystem providing internet of vehicles. *Sensors* **2019**, *19*, 550. [CrossRef] [PubMed]
11. Huch, S.; Ongel, A.; Betz, J.; Lienkamp, M. Multi-task end-to-end self-driving architecture for CAV platoons. *Sensors* **2021**, *21*, 1039. [CrossRef]
12. Ghiasi, A.; Li, X.; Ma, J. A mixed traffic speed harmonization model with connected autonomous vehicles. *Transp. Res. Part C Emerg. Technol.* **2019**, *104*, 210–233. [CrossRef]
13. Wang, X.; Park, S.; Han, K. Energy-Efficient Speed Planner for Connected and Automated Electric Vehicles on Sloped Roads. *IEEE Access* **2022**, *10*, 34654–34664. [CrossRef]
14. Sankar, G.S.; Kim, M.; Han, K. Data-driven Leading Vehicle Speed Forecast and its Application to Ecological Predictive Cruise Control. *IEEE Trans. Veh. Technol.* **2022**. [CrossRef]
15. Kim, W.; Noh, J.; Lee, J. Effects of vehicle type and inter-vehicle distance on aerodynamic characteristics during vehicle platooning. *Appl. Sci.* **2021**, *11*, 4096. [CrossRef]
16. Jacob, B.; de Chalendar, O.A. Truck platooning: Expected benefits and implementation conditions on highways. In *Heavy Vehicle Transportant Technology (HVTT) International Symposium*; 2018. Available online: <https://hvtforum.org/wp-content/uploads/2019/11/Jacob-TRUCK-PLATOONING-EXPECTED-BENEFITS-AND-IMPLEMENTATION-CONDITIONS-ON-HIGHWAYS.pdf> (accessed on 15 September 2022).
17. Jo, Y.; Kim, J.; Oh, C.; Kim, I.; Lee, G. Benefits of travel time savings by truck platooning in Korean freeway networks. *Transp. Policy* **2019**, *83*, 37–45. [CrossRef]
18. Sethuraman, G.; Liu, X.; Bachmann, F.R.; Xie, M.; Ongel, A.; Busch, F. Effects of bus platooning in an urban environment. In Proceedings of the 2019 IEEE Intelligent Transportation Systems Conference (ITSC), Auckland, New Zealand, 27–30 October 2019; pp. 974–980.
19. Lakshmanan, V.K.; Sciarretta, A.; Murlan, O.E.G. Cooperative Levels in Eco-Driving of Electric Vehicle Platoons. In Proceedings of the 2021 IEEE International Intelligent Transportation Systems Conference (ITSC), Indianapolis, IN, USA, 19–22 September 2021; pp. 1163–1170.
20. Hu, M.; Bauer, P. Energy Analysis of Highway Electric HDV Platooning Considering Adaptive Downhill Coasting Speed. *World Electr. Veh. J.* **2021**, *12*, 180. [CrossRef]
21. Prathiba, S.B.; Raja, G.; Dev, K.; Kumar, N.; Guizani, M. A hybrid deep reinforcement learning for autonomous vehicles smart-platooning. *IEEE Trans. Veh. Technol.* **2021**, *70*, 13340–13350. [CrossRef]
22. Polverino, P.; Arsie, I.; Pianese, C. Optimal energy management for hybrid electric vehicles based on dynamic programming and receding horizon. *Energies* **2021**, *14*, 3502. [CrossRef]
23. Gharib, A.; Stenger, D.; Ritschel, R.; Voßwinkel, R. Multi-objective optimization of a path-following MPC for vehicle guidance: A Bayesian optimization approach. In Proceedings of the 2021 European Control Conference (ECC), Delft, The Netherlands, 29 June 2021–July 2021; pp. 2197–2204.
24. Han, K.; Park, G.; Sankar, G.S.; Nam, K.; Choi, S.B. Model predictive control framework for improving vehicle cornering performance using handling characteristics. *IEEE Trans. Intell. Transp. Syst.* **2020**, *22*, 3014–3024. [CrossRef]
25. Serale, G.; Fiorentini, M.; Capozzoli, A.; Bernardini, D.; Bemporad, A. Model predictive control (MPC) for enhancing building and HVAC system energy efficiency: Problem formulation, applications and opportunities. *Energies* **2018**, *11*, 631. [CrossRef]
26. Amini, M.R.; Kolmanovsky, I.; Sun, J. Hierarchical MPC for robust eco-cooling of connected and automated vehicles and its application to electric vehicle battery thermal management. *IEEE Trans. Control Syst. Technol.* **2020**, *29*, 316–328. [CrossRef]
27. Lee, D.; Rousseau, A.; Rask, E. *Development and Validation of the Ford Focus Battery Electric Vehicle Model (No. 2014-01-1809)*; SAE Technical Paper; SAE International: Warrendale, PA, USA, 2014.

28. Long, H.; Khalatbarisoltani, A.; Hu, X. MPC-based Eco-Platooning for Homogeneous Connected Trucks Under Different Communication Topologies. In Proceedings of the 2022 IEEE Intelligent Vehicles Symposium (IV), Aachen, Germany, 4–9 June 2022; pp. 241–246.
29. Wang, F.; Zhuang, W.; Yin, G.; Liu, S.; Liu, Y.; Dong, H. Robust inter-vehicle distance measurement using cooperative vehicle localization. *Sensors* **2021**, *21*, 2048. [[CrossRef](#)] [[PubMed](#)]
30. Zabat, M.; Stabile, N.; Farascaroli, S.; Brow, F. *The Aerodynamic Performance of Platoons: A Final Report*; Escholarship: Los Angeles, CA, USA, 1995.
31. Guttenberg, M.; Sripad, S.; Viswanathan, V. Evaluating the potential of platooning in lowering the required performance metrics of li-ion batteries to enable practical electric semi-trucks. *ACS Energy Lett.* **2017**, *2*, 2642–2646. [[CrossRef](#)]
32. Hussein, A.A.; Rakha, H.A. Vehicle platooning impact on drag coefficients and energy/fuel saving implications. *IEEE Trans. Veh. Technol.* **2021**, *71*, 1199–1208. [[CrossRef](#)]
33. Hucho, W.H. (Ed.) *Aerodynamics of Road Vehicles: From Fluid Mechanics to Vehicle Engineering*; Elsevier: Amsterdam, The Netherlands, 2013.
34. Rousseau, A.; Pagerit, S.; DeLaughter, P.; Juskiewicz, M.; Sharer, P.; Vijayagopal, R. AMBER: A New Architecture for Flexible MBSE Workflows. In Proceedings of the 2017 IEEE Vehicle Power and Propulsion Conference (VPPC), Belfort, France, 11–14 December 2017; pp. 1–6.
35. Xu, Y.; Xu, K.; Wan, J.; Xiong, Z.; Li, Y. Research on particle filter tracking method based on Kalman filter. In Proceedings of the 2018 2nd IEEE Advanced Information Management, Communication, Electronic and Automation Control Conference (IMCEC), Xi'an, China, 25–27 May 2018; pp. 1564–1568.
36. Bhattacharyya, R.P. *Modeling Human Driving from Demonstrations*; Stanford University: Stanford, CA, USA, 2021.
37. Meiring, G.A.M.; Myburgh, H.C. A review of intelligent driving style analysis systems and related artificial intelligence algorithms. *Sensors* **2015**, *15*, 30653–30682. [[CrossRef](#)]
38. Simon, D. *Optimal State Estimation: Kalman, Hinfinitiy, and Nonlinear Approaches*; John Wiley Sons: Hoboken, NJ, USA, 2006.
39. Lisle, R.J. Google Earth: A new geological resource. *Geol. Today* **2006**, *22*, 29–32. [[CrossRef](#)]